Materialia 9 (2020) 100521

Contents lists available at ScienceDirect

Materialia

journal homepage: www.elsevier.com/locate/mtla

Full Length Article

Superplasticity in fine grained dual phase high entropy alloy

S.S. Nene, K. Liu, S. Sinha, M. Frank, S. Williams, R.S. Mishra*

Center for Friction Stir Processing, Department of Materials Science and Engineering, University of North Texas, Denton, TX 76207, USA

ARTICLE INFO

Keywords:
Dual phase HEA
Superplasticity
Strain rate sensitivity
Grain boundary sliding
Cavitation
Diffusion creep

ABSTRACT

$Fe_{42}Mn_{28}Co_{10}Cr_{15}Si_5$ high entropy alloy (DP-5Si-HEA) exhibited superplastic elongation of 550% at $\dot{\varepsilon} = 10^{-3}s^{-1}$ after complete tensile deformation at 700 °C. Pronounced Cr partitioning at testing temperature facilitated σ phase formation which assisted in stabilizing the grain size during deformation. Stable equiaxed fine-grained dual phase microstructure at all strain rates suggested dominance of grain boundary sliding over diffusion creep to maintain the superplasticity at the tested strain rate-temperature combinations. Cavitation along the gage region is evident, however, effective diffusional linkage of the cavities along the superplastic flow resulted in elongations >200% irrespective of strain rate at 700 °C.

1. Introduction

Dual phase high entropy alloys (DP-HEAs) have gained interest in recent times due to their ability to exhibit higher strength-ductility synergy at room temperature. This mechanical response in DP-HEAs is attributed to strain accommodation via multiple deformation mechanisms such as transformation ($\gamma \rightarrow \varepsilon$) induced plasticity (TRIP) and twinning based on the prior γ (f.c.c.) and ε (h.c.p.) phase fractions and grain sizes [1–4]. However, the transformation effect weakens with increase in temperature in conventional TRIP steels owing to thermodynamically favorable γ phase stabilization [5]. Hence, understanding the deformation response of these DP-HEAs at elevated temperatures is of interest.

High-temperature deformation response is characterized by strain rate dependence on grain size exponent (p) and stress exponent (n) for a given temperature [6]. In general, values of p and n govern deformation mechanism at elevated temperatures, and most dislocation related mechanisms show $n > 2$ and $p = 0$, whereas superplastic deformation exhibits $n = 2$–3 and $p > 0$ [6–9]. The operative deformation mechanisms can be predicted by determination of strain rate sensitivity ($m = n^{-1}$) at a given temperature for a defined strain rate range. Classic literature on superplasticity in conventional materials has established that higher m value in the range of 0.3–0.5 can be attained in the materials having grain sizes less than 10 μm at elevated temperature, which retards flow localization and promotes superplasticity. However, it is necessary to stabilize the fine grain size during high temperature deformation and hence superplastic deformation is claimed to be favorable in two-phase microstructures having equal fractions or in microstructures having thermally stable precipitates pinning the grain boundaries [6–9].

First report on superplastic elongation in HEAs is made by Kuznetsov et al. [10] for forged AlCrCuNiFeCo HEA showing maximum tensile elongation of 860% at 1000 °C, 10^{-3} s^{-1} which they attributed to formation of f.c.c. and b.c.c. containing fine grained equiaxed microstructure during deformation [10]. Further, Reddy et al. [11] claimed superplastic elongation of ~320% in equiatomic CoCrFeMnNi HEA at 750 °C, 10^{-4} s^{-1} due to the refined quasi-single phase microstructure that evolved after thermo-mechanical processing. Zhang et al. [12] reported ultrahigh ductility of ~250% in eutectic HEA $AlFeCoCrNi_{2.1}$ at 1000 °C, 10^{-3} s^{-1} whereas Shaysultanov et al. [13] reported almost 1240% tensile elongation in AlCoCrCuFeNi equiatomic HEA at 1000 °C, 10^{-2} s^{-1} after multi-axial forging owing to the simultaneous precipitation and recrystallization events during high-temperature deformation.

The present work aims in further understanding of the deformation response of one of the DP- HEAs having composition $Fe_{42}Mn_{28}Co_{10}Cr_{15}Si_5$ (all in at%, hence forth designated as DP-5Si-HEA) at various quasistatic strain rates and temperatures in fine-grained condition. Ultrafine grain microstructure was obtained by friction stir processing (FSP) of DP-5Si-HEA and deformation behavior was studied at tested strain rates and temperature with respect to operational strain accommodation mechanisms and was subsequently correlated with the concurrent microstructural evolution.

2. Experimental

DP-5Si-HEA was fabricated by casting in a vacuum induction melting furnace with nominal composition and subsequent rolling at 900 °C, to achieve 50% reduction. To relieve the stresses and maintain chemical homogeneity, the plate was then homogenized at 1200 °C for 1 hr followed by water quenching. A rectangular piece of 160 × 75 × 12.5 mm^3 was cut from the rolled plate and friction stir

* Corresponding author.
E-mail address: rajiv.mishra@unt.edu (R.S. Mishra).

https://doi.org/10.1016/j.mtla.2019.100521
Received 3 September 2019; Accepted 26 October 2019
Available online 1 November 2019

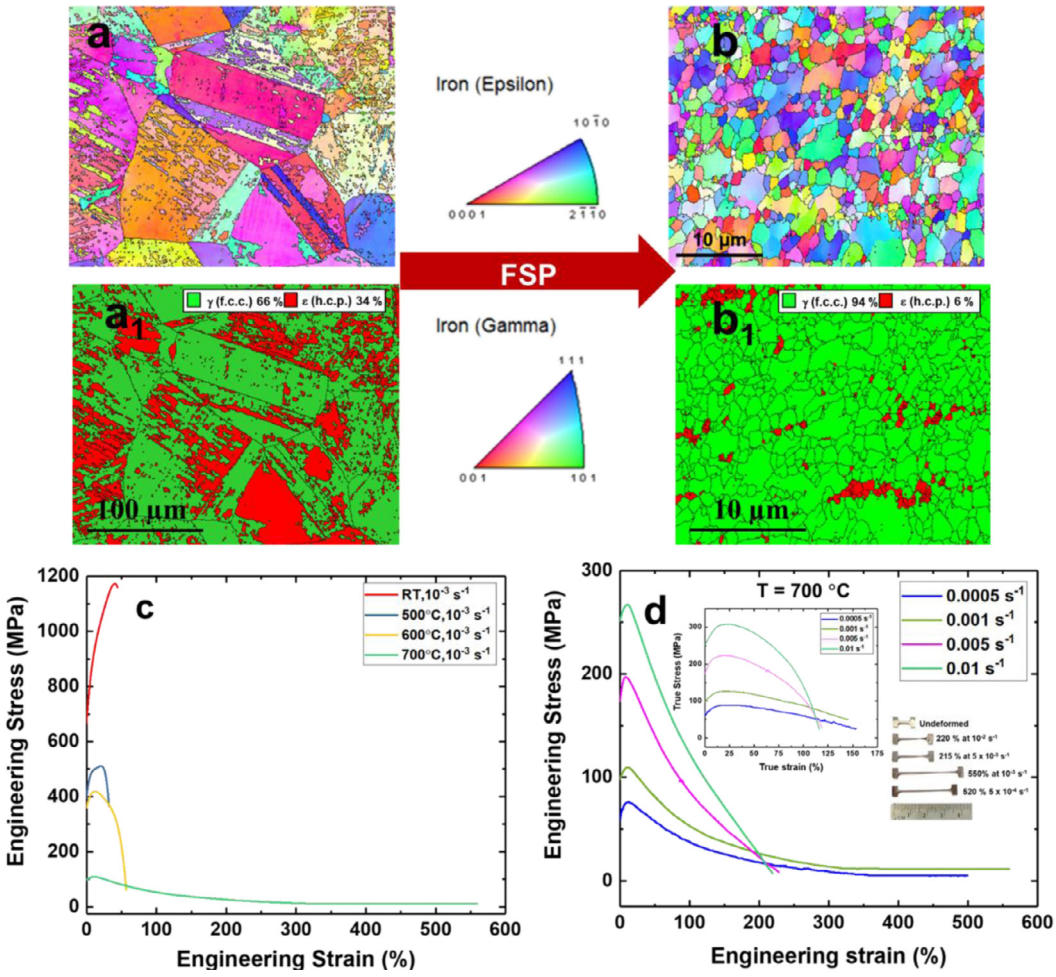

Fig. 1. EBSD IPF maps for (a) as-cast condition, (b) as-FSP condition, EBSD phase maps for (a_1) as-cast condition, (b_1) as-FSP condition, (c) engineering stress-engineering strain curves for as-FSP condition at $\dot{\varepsilon} = 10^{-3}s^{-1}$ for different temperatures, (d) engineering stress-engineering strain curves (inset: true stress-true strain curves) for as-FSP condition at 700 °C for different strain rates. (EBSD: electron backscattered diffraction: IPF: inverse pole figure; FSP: friction stir processing).

processed using a W-Re tool with tool rotational rate of 150 rotations per minute (RPM), transverse speed of 2 inches per minute (IPM) and at tilt angle of 2.0°. A Cu backing plate was used for effective heat dissipation, and Ar was blown near the specimen tool interface to avoid oxygen pickup during processing. The processing tool had a shoulder diameter of 12 mm with a tapered pin. The root diameter, pin diameter, and length of the tool were 7.5 mm, 6 mm, and 3.5 mm, respectively.

Metallographic specimens for all conditions (as-cast, as-FSP, deformed) were prepared starting from 600 grade emery paper polishing followed by final polishing with 0.02 μm colloidal silica. Microstructures for all these conditions were analyzed by Electron backscatter diffraction (EBSD) measurements carried out on FEI NOVA Nano-SEM with a Hikari camera, and the data were analyzed using TSL OIM 8 software. As the grain size attained during FSP was significantly fine, EBSD scans were performed at magnifications of 2000 X and 6000 X. To capture sufficient grains during high magnification scans (6000 X), grain size and phase fractions were estimated at three different locations, and the average values have been reported. X-ray microscopy (XRM) of selected fractured tensile specimen was performed using Zeiss Xradia Versa 520 microscope. The XRM scan was carried out at 80 kV and 7 W, using source to sample distance of 15 mm and sample to detector distance of 21 mm. A 20X objective, binning = 4, exposure = 10 s, angular range of 360° and 3601 projections were used. Dragonfly software was used to analyze the XRM data. X-ray diffraction (XRD) measurements were performed using an RIGAKU X-Ray equipment equipped with Cu K_α radiation operated at 40 kV and 30 mA.

Rectangular 1 mm-thick, dog-bone-shaped mini-tensile specimens were machined using a computer numerical control (CNC) machine from 1 mm below the surface within the nugget region of FSP specimens; gage length and width of the tensile specimens were 5 and 1.25 mm, respectively. High-temperature tensile tests were carried out by heating the mini tensile specimen in 3 zone ATS heating furnace at 500, 600, 625, 650, 675 and 700 °C and at constant initial strain rates of 0.0005, 0.001, 0.005, 0.01 s^{-1}. Before starting the tests, the specimens were soaked for 5–7 min at test temperature.

3. Results and discussion

Fig. 1a and b shows the EBSD inverse pole figure (IPF) maps whereas Fig. 1a_1 and b_1 shows the phase maps for as-cast and as-FSP (single FSP run carried out at 150 RPM) conditions, respectively. As expected, FSP resulted in extremely refined equiaxed microstructure ($d_{avg} = 0.7$ μm) having ~88% γ and 12% ε phase fractions (Fig. 1a–b_1). Thus, the grain-refined γ phase dominant as-FSP microstructure was selected for tensile tests as a function of temperature and strain rates.

Fig. 1c shows the engineering stress-engineering strain curves for DP-5Si-HEA after complete tensile deformation as a function of temperature at $\dot{\varepsilon} = 10^{-3}s^{-1}$. Temperature-dependent flow softening is evident by the drop in flow stress with increase in temperature. Room-temperature elongation, however, was comparable with the intermediate temperature (500 and 600 °C) ductility owing to the extremely high work hardening ability of as-FSP DP-5Si-HEA [2,4]. The

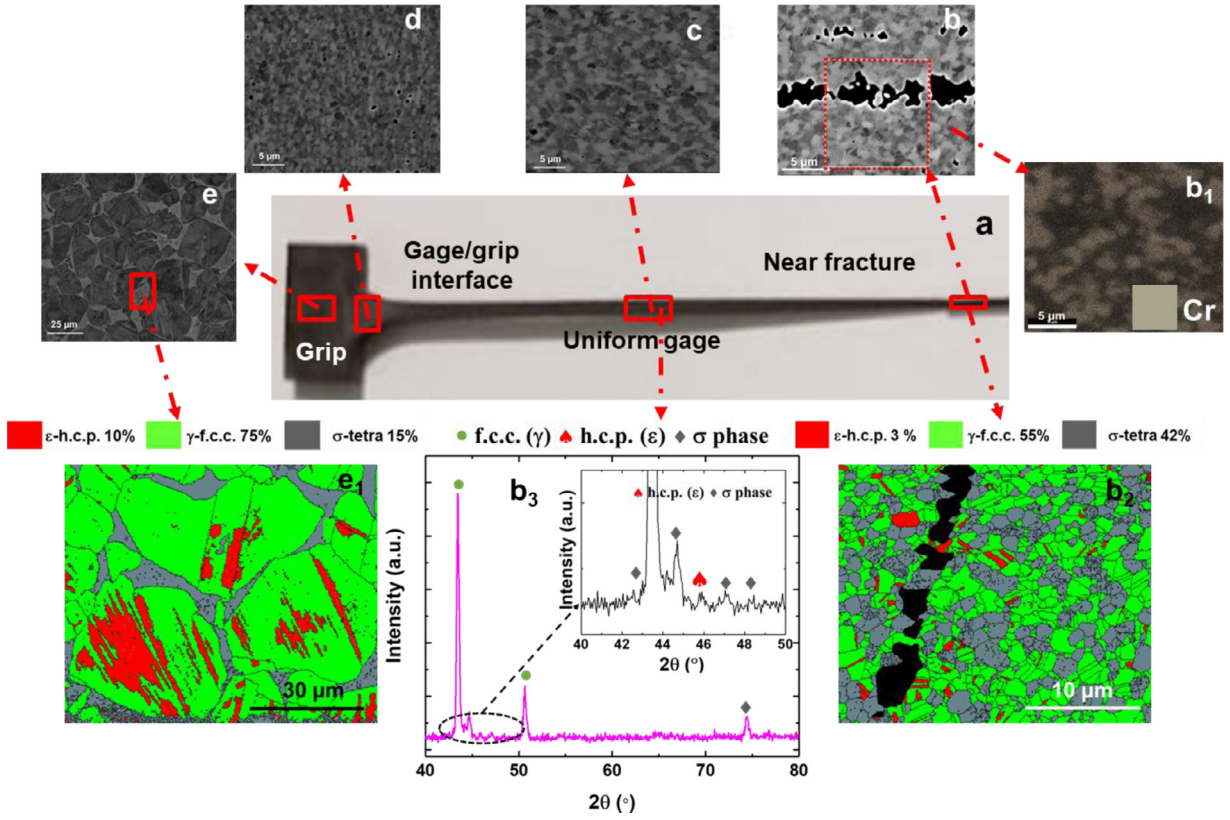

Fig. 2. (a) Optical image of the superplastically deformed specimen at 0.001 s^{-1} and 700 °C, (b) back scattered electron image of the near fracture region, (b_1) EDS-X-ray map corresponding to (b), (b_2) EBSD phase map of the near fracture region, (b_3) X-ray diffraction map near the fracture region showing formation of sigma phase (c) back scattered electron image in uniform gage region, (d) back scattered electron image at gage/grip interface, and (e) back scattered electron image in middle of the grip, (e_1) EBSD phase map in the grip region, (EBSD: electron backscattered diffraction: IPF: inverse pole figure; EDS: energy dispersive spectroscopy).

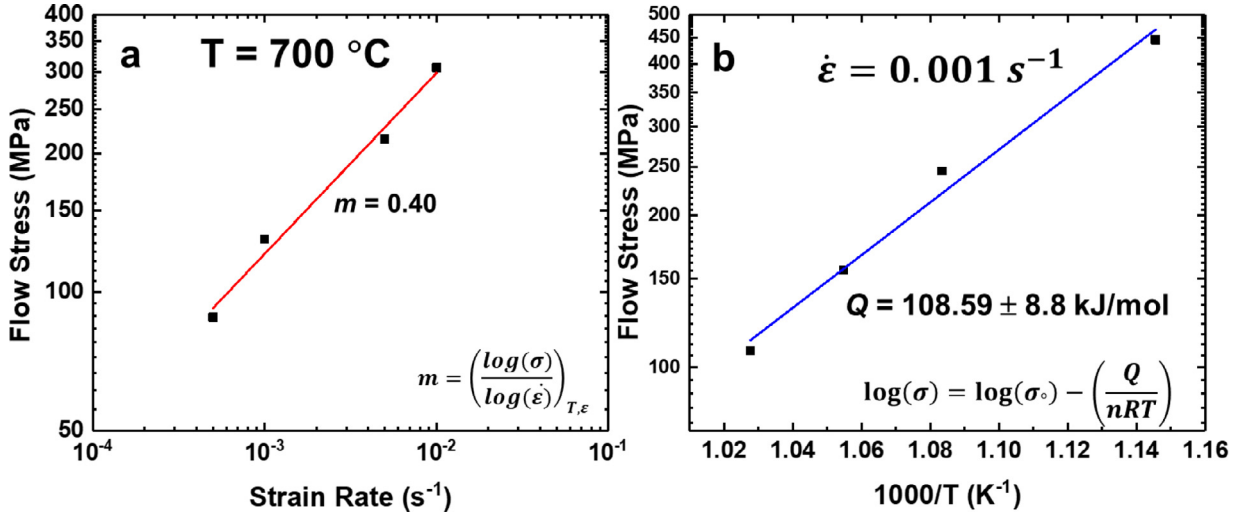

Fig. 3. (a) Flow stress–strain rate plot for estimation of strain rate sensitivity (m) at 700 °C, and (b) flow stress-temperature plot for estimation of activation energy at $\dot{\varepsilon} = 0.001\ s^{-1}$.

green curve in Fig. 1c depicts evidence of superplastic like flow in the material when deformed at 700 °C at $\dot{\varepsilon} = 10^{-3}s^{-1}$ showing total elongation of ~550%. The specimens were air-cooled after each tensile test at higher temperature to investigate microstructural evolution at different regions of the tensile specimen. As the as-FSP specimen displayed exceptional elongation at 700 °C, this temperature was chosen to further study deformation behavior as a function of strain rates. Fig. 1d displays the engineering stress-engineering strain curves for the as-FSP condition as a function of strain rate. Flow stress dependence on strain rate is evident and points towards high strain rate sensitivity (SRS) at test temperature. Flow softening is also seen in all specimens irrespective of strain rate as captured in true stress-true strain curves shown in Fig. 1(d) inset. However, the extent of flow localization appears to be increased with strain rate. This relatively higher flow softening effect for specimens tested at higher strain rates is attributed to the pronounced cavitation in these specimens as a result of higher flow stress imparted during defor-

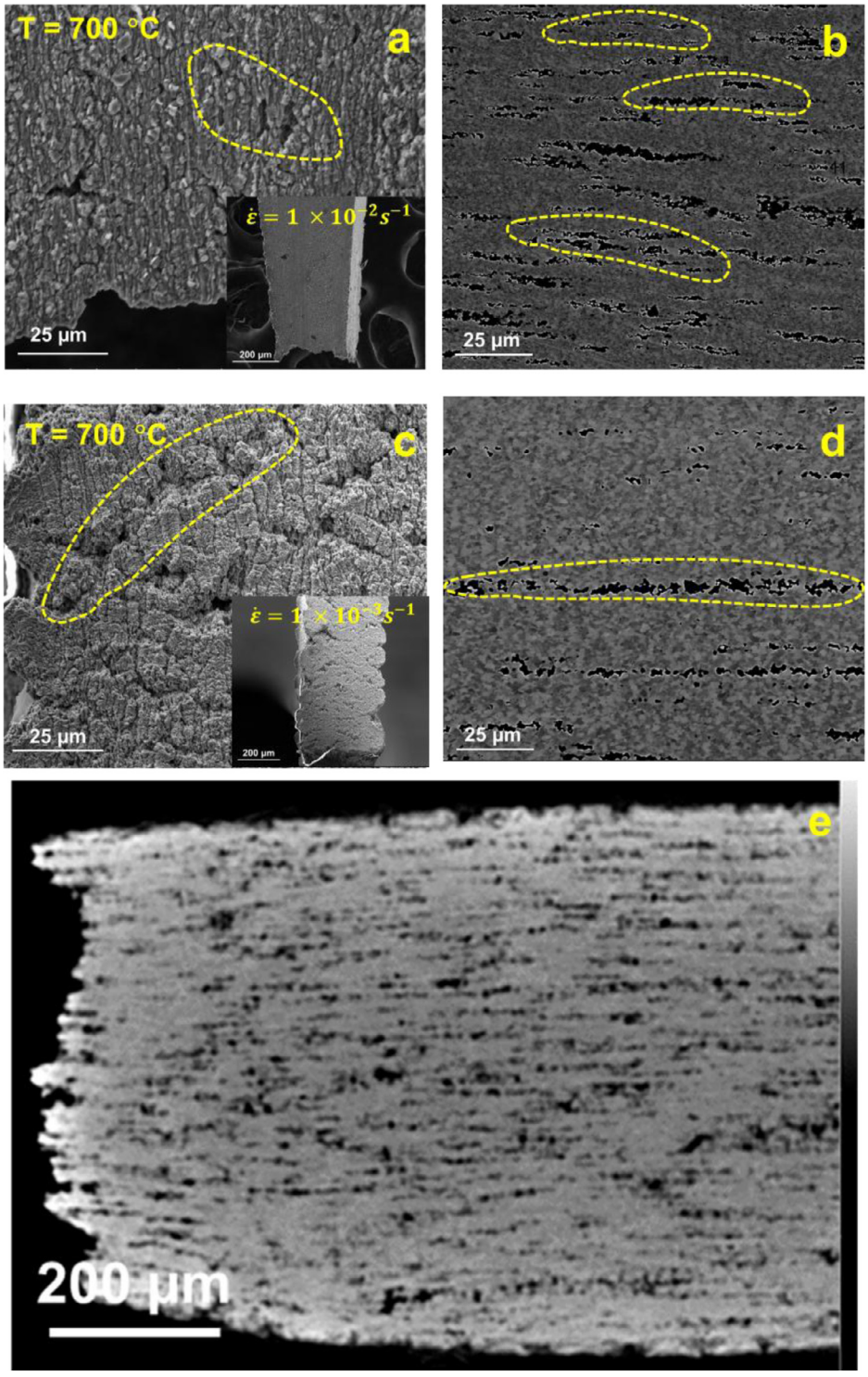

Fig. 4. Secondary electron images showing (a) formation of cavities along the gage near fracture region in unpolished condition (inset: overall gage displaying no visible necking), (b) ductile fracture showing very fine dimples in 10^{-2} s^{-1} specimen, (c) formation of cavities along the gage near fracture region in unpolished condition (inset: overall gage displaying visible necking), (d) ductile fracture showing very fine dimples in 10^{-3} s^{-1} specimen, and (e) X-ray microscopy image showing cavitation throughout the volume of the specimen deformed at 10^{-3} s^{-1}.

mation [6–7]. The detail of cavitation is briefly explained in subsequent section.

Fig. 2a–e_3 captures the microstructural evolution in a specimen deformed at 1×10^{-3} s^{-1} at 700 °C for different regions namely, near fracture, uniform gage (uniformly deformed region) and grip (unaffected by deformation). As expected, region close to fracture showed an extremely refined multi-phase microstructure (Fig. 2b–b_1) comprised of 42% σ, 55% γ and marginal ε phases. As reported in duplex stainless steels and Cr-rich steels [13–16], significant Cr partitioning that occurs at 700 °C leads to σ formation, which is also seen in the present alloy as depicted in EDS X-ray maps as well as EBSD and X-ray diffraction (XRD) results (Fig. 2b–b_3). The occurrence of σ precipitation at 700 °C during deformation is dependent on time available for Cr partitioning in Fe-Cr-Si containing matrix [14].

The σ phase formation is more favored kinetically in the Fe–Cr–Si system than in the Fe–Cr binary system; and as a result, the σ phase formation becomes prevalent in DP-5Si-HEA with increased elongation during tensile testing, as it provides more driving force for Cr partitioning [13–16]. The σ phase is also known to be stronger than the γ matrix at higher temperature. Additionally, it can hinder grain growth, thereby maintaining the microstructural stability required for superplastic deformation [6–9]. Therefore, σ formation during hot deformation

maintained extremely fine-grained equiaxed microstructure during superplastic flow throughout the gage of the deformed specimen as evident in Fig. 2b$_2$, c and d. It is also important to note that formation of ε (h.c.p.) phase is not expected in DP-5Si-HEA at the test temperature of 700 °C, because this is well above the critical temperature for $\gamma \rightarrow \varepsilon$ transformation (~ 425 °C) [2]. Any observation of ε (h.c.p.) phase is superplastic tested specimen after cooling to room temperature (as evident in Fig. 2b–d) is because of $\gamma \rightarrow \varepsilon$ transformation during cooling. As a result, Figs. 1c, d and 2b–d together confirms superplasticity in as-FSP condition of DP-5Si-HEA at 700 °C.

Also it is important to note that, the microstructure evolved at grip clearly showed coarse grain structure with exceptional Cr partitioning (Fig. 2e, e$_1$). Grip being statically heated during the entire testing time, the microstructure gets exposed to the testing temperature for the maximum period, which accelerates σ formation kinetically (Fig. 2e, e$_1$). On a similar note, the fraction of σ phase formed in the specimen deformed at 10^{-3} s^{-1} was compared with the fraction formed in 10^{-2} s^{-1} specimen after tensile testing; and, as expected, faster strain rate showed lower σ formation (~31% σ phase) than slower strain rate of 10^{-3} s^{-1} (42% σ) due to lesser time available for Cr diffusion in the former. In short, σ formation was crucial in providing microstructural stability during superplastic flow, thereby showing almost submicron grain size throughout the gage region.

To understand deformation accommodation during superplastic deformation, flow stress values at intermediate strain of 10% were obtained from true stress-true strain curves and were plotted with strain rate to obtain strain rate sensitivity index (m) (Fig. 3a). Fig. 3a confirms that DP-5Si-HEA exhibited a high m value of 0.4 within the strain rate regime of 10^{-4}–10^{-2} s^{-1} at 700 °C. The higher m value (0.3–0.5) corresponding to stage II in the classic SRS plot for metals [8,9,11] points towards activation of grain boundary sliding (GBS) during deformation. Moreover, the m value of 0.4 coincides with the stress exponent (n) of 2.5, which is also comparable with the theoretical n value (~2) predicted for grain boundary sliding [6–8,16]. It is postulated that, higher elongations in the material are either due to diffusion creep or by GBS and the distinguishing feature is the microstructural evolution after superplastic flow. Diffusion creep leads to elongated grains in the gage region due to extensive diffusion along the boundaries whereas GBS shows traditional fine grained equiaxed microstructure at the testing temperature and strain rate. Thus, along with the m value, the equiaxed microstructural evolution in the gage region (Fig. 2b–d) confirms GBS as the primary mechanism of superplastic deformation in the 10^{-3} s^{-1} specimen [17].

Activation energy (Q) for the deformation was estimated for the as-FSP to be 108.6 kJ/mol. This value of Q is close to the grain boundary (163 kJ/mol) diffusion activation energy reported in literature for γ-iron [18]. Generally, the Q value for most conventional alloys under the superplastic temperature regime is near to the Q value for grain boundary diffusion [6–9,16]. However, testing temperatures used in the current work are very sensitive to either ε or σ formation. Lower testing temperatures promote the former, whereas the latter dominates at higher testing temperatures and hence may alter the overall kinetics of superplastic flow. Thus, Q value was calculated by doing tensile tests within the controlled intervals of temperature in superplastic regime (600, 650, 675 and 700 °C) for the alloy to avoid any effect of phase transformations.

Fig. 4a–d displays the fracture behavior for the 10^{-2} s^{-1} and 10^{-3} s^{-1} specimens. Irrespective of strain rates, both specimens showed traditional cavitation near the fracture surface which also confirms that the diffusive phenomena dominate the superplastic flow in this material (Fig. 4a and c). However, it is important to note that, the extent of cavity formation is higher in 10^{-2} s^{-1} specimen than 10^{-3} s^{-1} as confirmed by Fig. 4b and d, respectively. Cavities are formed mainly by stress concentration imposed during GBS on grain or phase boundary, thereby causing failure via nucleation and growth [6,8,17–20]. Thus, higher the interfacial area available in terms of grain or phase boundary, higher will be cavity formation [6,8,16–19]. However, maintaining the superplastic flow via diffusional cavity linkage demands cavity size greater than the grain size during deformation [20]. Therefore, 10^{-3} s^{-1} specimen displayed very dominant cavity linkage near the fracture as highlighted in Fig. 4d due to higher cavity size (5–6 μm) than the equiaxed grain size < 1 μm. Moreover, Fig. 2b$_2$ clearly show diffusional cavity linkage occurred in the 10^{-3} s^{-1} specimen, delaying the fracture significantly and hence showed substantial superplastic elongation of 550%. Moreover, this linkage of cavities was also confirmed by doing the X-ray microscopy (XRM) which captures the cavitation throughout the volume of the specimen. Fig. 4e displays such XRM image which not only shows formation of cavities but also their diffusional linkage along the gage.

In the case of high strain rate specimen, the presence of very fine grained equiaxed microstructure shows that the higher elongation attained is mainly due to GBS and not by diffusional creep [17–20]. Further, though the cavitation is distinct in the 10^{-2} s^{-1} specimen, cavity linkage was limited in spite of having cavity size greater than grain size. This is mainly attributed to the fact that cavity nucleation ($\dot{N} = \exp(-\frac{\gamma^3}{\sigma^2 kT})$, where, $\dot{N}$ = cavity nucleation rate, γ = surface energy, σ = flow stress) was faster in this specimen due to higher flow stress associated with the deformation and presence of number of γ/σ interphase boundaries due to finer grain size (Fig. 4c) [20]. As a result, there are islands of cavities formed in 10^{-2} s^{-1} specimen (highlighted by yellow dotted circles in Fig. 4c) which are inadequate for maintaining the superplastic flow in the material for attaining larger elongation. In short, notable σ formation maintained the equiaxed dual phase microstructure which facilitated the GBS at the testing temperature and strain rates in DP-5Si-HEA, however, lower flow stress values at slower strain rates promoted effective cavity linkage required for prolonged superplastic flow [18–20]. Thus, this microstructural evolution in combination with the higher elongations obtained at 700 °C shows evidence of superplasticity in as-FSP condition of DP-5Si-HEA which is desirable for most of the superplastic forming applications.

4. Conclusions

In summary, friction stir processed DP-5Si-HEA displayed exceptional superplastic elongation at relatively higher strain rates. The ability of the material to exhibit σ formation at higher temperature provides exceptional ductility of > 200% at 700 °C irrespective of strain rate. The formation of σ phase facilitated microstructural stability enabled grain boundary sliding during deformation with strain rate sensitivity (m) of 0.4. Increase in grain and phase boundaries due to γ and σ phase containing dual phase microstructure triggered cavitation whereas these cavities merged together via diffusional cavity linkage at testing temperature in a specimen deformed at slower strain rate.

Declaration of Competing Interest

The authors declare that they have no known competing financial interests or personal relationships that could have appeared to influence the work reported in this paper.

Acknowledgments

The work was carried out under the cooperative agreement of the University of North Texas with U.S. Army Research Laboratory (W911NF-18-2-0067). The authors thank Materials Research Facility (MRF) at University of North Texas for access to microscopy facilities. The authors also acknowledge Mr. Christopher Morphew and Ms. Advika Chesetti for their help in preparation of metallographic specimens.

References

[1] S.S. Nene, K. Liu, M. Frank, R.S. Mishra, R.E. Brennan, K.C. Cho, Z. Li, D. Raabe, Enhanced strength and ductility in a friction stir processing engineered dual phase high entropy alloy, Sci. Rep. 7 (2017) 16167.

[2] S.S. Nene, K. Liu, M. Frank, R.S. Mishra, B.A. McWilliams, K.C. Cho, Extremely high strength and work hardenability in metastable high entropy alloy, Sci. Rep. 8 (2018) 9920.
[3] S.S. Nene, M. Frank, K. Liu, S. Sinha, R.S. Mishra, B.A. McWilliams, K.C. Cho, Reversed strength-ductility relationship in microstructurally flexible high entropy alloy, Scr. Mater. 154 (2018) 163.
[4] K. Liu, S.S. Nene, M. Frank, S. Sinha, R.S. Mishra, Metastability assisted fatigue behavior in friction stir processed dual phase high entropy alloy, Mater. Res. Lett. 6 (2018) 613.
[5] S. Curtze, V.-T. Kuokkala, M. Hokka, P. Peura, Deformation behavior of TRIP and DP steels in tension at different temperatures over a wide range of strain rates, Mater. Sci. Eng. A 507 (2009) 124.
[6] M.E. Kassnera, M.T. Pérez-Pradoa, Five-power-law creep in single phase metals and alloys, Prog. Mater. Sci. 45 (2000) 1–102.
[7] R.S. Mishra, M.W. Mahoney, S.X. McFadden, N.A. Mara, A.K. Mukherjee, High strain rate superplasticity in a friction stir processed 7075 Al alloy, Scr. Mater. 42 (2000) 163.
[8] S.S. Nene, G. Sharma, R.N. Singh, B.P. Kashyap, Microstructural evolution in and flow properties of Zr–2.5Nb pressure tube material at elevated temperature, J. Nucl. Mater. 449 (2014) 62.
[9] B.P. Kashyap, A. Arieli, A.K. Mukherjee, Microstructural aspects of superplasticity, J. Mater. Sci. 20 (1985) 2661.
[10] A.V. Kuznetsov, D.G. Shaysultanov, N.D. Stepanov, G.A. Salishchev, O.N. Senkov, Tensile properties of an AlCrCuNiFeCo high-entropy alloy in as-cast and wrought conditions, Mater. Sci. Eng. A 533 (2012) 107.
[11] S.R. Reddy, S. Bapari, P.P. Bhattacharjee, A.H. Chokshi, Superplastic-like flow in a fine-grained equiatomic CoCrFeMnNi high-entropy alloy, Mater. Res. Lett. 5 (2017) 408.
[12] Y. Zhang, X. Wang, J. Li, Y. Huang, Y. Lu, X. Sun, Deformation mechanism during high-temperature tensile test in an eutectic high-entropy alloy $AlCoCrFeNi_{2.1}$, Mater. Sci. Eng. A 724 (2018) 148.
[13] D.G. Shaysultanov, N.D. Stepanov, A.V. Kuznetsov, G.A. Salishchev, O.N. Senkov, Phase Composition and Superplastic Behavior of a Wrought AlCoCrCuFeNi High--Entropy Alloy, JOM 65 (2013) 1815.
[14] M. Sagradi, D. Pulino Sagradi, R.E. Medrano, The effect of the microstructure on the superplasticity of a duplex stainless steel, Acta Mater. 46 (1998) 3857.
[15] C.C. Hsieh, W. Wu, Overview of Intermetallic Sigma (σ) Phase Precipitation in Stainless Steels, doi:10.5402/2012/732471.
[16] H. Zhang, B. Bai, D. Raabe, Superplastic martensitic Mn–Si–Cr–C steel with 900% elongation, Acta Mater. 59 (2011) 5787.
[17] M. Kawasaki, T.G. Langdon, Principles of superplasticity in ultrafine-grained materials, J. Mater. Sci. 42 (2007) 1782.
[18] K.A. Padmanabhan, S. Balasivanandha Prabu, R.R. Mulyukov, A. Nazarov, R.M. Imayev, S. Ghosh Chowdhury, Superplasticity, Superplasticity, Springer, Berlin, Germany, 2018.
[19] H.J. Frost, M.F. Ashby, Deformation Mechanism Maps, Deformation Mechanism Maps, Pergamon Press, New York, 1982.
[20] A.H. Chokshi, T.G. Langdon, A model for diffusional cavity growth in superplasticity, Acta Metal. 35 (1987) 1089.